npj | quantum materials

Article

Published in partnership with Nanjing University

https://doi.org/10.1038/s41535-024-00653-3

Large anomalous Hall effect in spin fluctuating devil's staircase

Naoki Abe[1], Yuya Hano[1], Hiroaki Ishizuka[2], Yusuke Kozuka[3], Terumasa Tadano[4], Yoshihiro Tsujimoto[3], Kazunari Yamaura[3], Shintaro Ishiwata[5,6] & Jun Fujioka[1,7]

Electrons in metals can show a giant anomalous Hall effect (AHE) when interacting with characteristic spin texture. The AHE has been discussed in terms of scalar-spin-chirality (SSC) in long-range-ordered noncollinear spin textures typified by Skyrmion. The SSC becomes effective even in the paramagnetic state with thermal fluctuations, but the resultant AHE has been limited to be very small. Here, we report the observation of large AHE caused by the spin fluctuation near the devil's staircase transition in a collinear antiferromagnetic metal $SrCo_6O_{11}$. The AHE is prominent near and above the transition temperature at moderate magnetic fields, where the anomalous Hall angle becomes the highest level among known oxide collinear ferromagnets/antiferromagnets (>2%). Furthermore, the anomalous Hall conductivity is quadratically scaled to the conductivity. These results imply that the thermally induced solitonic spin defects inherent to the devil's staircase transition promote SSC-induced skew scattering.

Exploration of nontrivial spin textures in magnetic metals and semiconductors is a subject of great interest in modern condensed matter science. The striking feature is that conduction electrons interacting with the spin texture often cause unprecedented electromagnetic phenomena through the quantal phase. One of the typical examples is the anomalous Hall effect (AHE)[1]. Conventionally, the AHE has been considered to be induced by the spontaneous magnetization in ferromagnets but is currently observed even in a variety of antiferromagnets and helimagnets[2–7]. For example, helimagnets such as magnetic Skyrmions show the AHE or topological Hall effect in proportion to the scalar-spin chirality (SSC) $S_i \cdot (S_j \times S_k)$, which represents the solid angle formed by three spins in a noncoplanar configuration[8–12]. From a microscopic viewpoint, this effect is usually understood from the scheme of Berry curvature for electrons; the Berry curvature (quantal phase) proportional to the SSC is induced by the long-range ordered noncoplanar spin texture, which acts as the fiction magnetic field to conduction electrons[1]. In particular, it has been demonstrated that the Hall response can be remarkably enhanced by tuning the real space and/or momentum space Skyrmion density[13,14]. The giant anomalous/topological Hall response has also received interest in terms of spintronic function such as the efficient electrical read-out of spin texture or thermoelectric energy harvesting[15,16].

On the other hand, the AHE can be also triggered by fluctuating or spatially inhomogeneous spin texture that is not long-range ordered. For example, electron scattering from a single magnetic defect causes the AHE of skew scattering or side-jump mechanism[17,18]. In addition, it is also known that the transient noncoplanar spin texture induced by the thermal spin fluctuation triggers the AHE through the SSC. This phenomenon has been often understood from the scheme of Berry curvature mechanism[1,12], but recent research proposes that the multiple skew scattering from spin clusters with noncoplanar spin texture can cause the giant AHE[18,19], the anomalous Hall angle ($\tan\theta_H$) of which is scaled to the SSC. In particular, for the latter cases, the anomalous Hall angle comparable to or larger than the intrinsic AHE of Skrmion magnets can emerge even in the paramagnetic temperature regime far above the magnetic transition temperature[20]. This is in contrast with the conventional intrinsic/extrinsic AHE, which is usually enhanced in the long-range ordered state. Nevertheless, the AHE originating from spin fluctuations i.e. paramagnetic AHE is usually very small in most magnetic metals ($\tan\theta_H \leq 0.01$)[12,21–28] except in a few noncollinear magnets[20,21]. Here, we report that the collinear antiferromagnetic metal

[1]Graduate School of Science and Technology, University of Tsukuba, Tsukuba, Ibaraki 305-8573, Japan. [2]Department of Physics, Tokyo Institute of Technology, Meguro, Tokyo 152-8551, Japan. [3]Research Center for Materials Nanoarchitechtonics (MANA), National Institute for Materials Science (NIMS), Namiki, Tsukuba, Ibaraki 305-0044, Japan. [4]Research Center for Magnetic and Spintronic Materials (CMSM), National Institute for Materials Science (NIMS), Sengen, Tsukuba, Ibaraki 305-0047, Japan. [5]Division of Materials Physics, Graduate School of Engineering Science, Osaka University, Osaka 560-8531, Japan. [6]Spintronics Research Network Division, Institute for Open and Transdisciplinary Research Initiatives, Osaka University, Suita, Osaka 565-0871, Japan. [7]Department of Materials Science, University of Tsukuba, Tsukuba, Ibaraki 305-8573, Japan. e-mail: fujioka@ims.tsukuba.ac.jp

$SrCo_6O_{11}$ with devil's staircase-type transition shows the large paramagnetic AHE in a moderate magnetic field (~3 T) even far above the magnetic transition temperature, resulting in the anomalous Hall angle ($\tan\theta_H$) more than 0.02.

Results

Magnetic property

$SrCo_6O_{11}$ crystallizes in the *R*-type hexaferrite structure with space group $P6_3/mmc$[29]. In this material, the Co-sublattice can be viewed as the stacking of Kagome lattice of Co1, dimerized pillar of Co2, and triangular lattice of Co3 along the *c*-axis as shown in Fig. 1a. The Co1 and Co2 form the CoO_6-octahedra, while the Co3 does the CoO_5-bipyramids as illustrated in Fig. 1b, c, respectively. The 3*d* states of Co3 form a local spin moment with easy-axis anisotropy along the *c*-axis, while those of Co1 and Co2 take the partially filled low spin states, yielding the strongly correlated conduction electrons[30–33] [see also Supplementary Fig. 1]. The conduction electrons mediate the magnetic interaction of Co3-spin through the Ruderman-Kittel-Kasuya-Yoshida (RKKY)-type interaction, resulting in the competing multiple magnetic interactions between the nearest-neighbor spins and further-neighbor spins along the *c*-axis[34]. Consequently, the collinear antiferromagnetic phases, in which spins are modulated along the *c*-axis but are ferromagnetically aligned within the *ab*-plane, occur at low temperatures. As an example, Fig. 1a shows the magnetic structure with the modulation wave number $q = 1/3$, where spins are aligned in the c-direction in an up-up-down order.

Figure 1d shows the magnetic phase diagram when the magnetic field (*B*) is applied along the *c*-axis. At zero magnetic field, the magnetic ordering with incommensurate (IC) modulation $q \sim 1/5$ appears at 22 K ($= T_c$). With lowering temperature, *q* quasi-continuously decreases and is locked to the commensurate value of 1/6 about 12 K[34]. Simultaneously, various magnetic phases with different modulation periods emerge, resulting in the phase-separated state. When the magnetic field is applied along the *c*-axis, these states change to the $q = 1/3$-phase at B_{c1}, followed by the forced ferromagnetic phase at B_{c2}. These field-induced phase transitions can be seen as the magnetization jumps and plateaus as shown in the inset to Fig. 1d[33,34] (see also Fig. 2a–d). Such behavior is a hallmark of the magnetic devil staircase, which originates from the competition among a large number of nearly degenerate magnetic phases with different modulation period[35,36].

Magneto-transport property

Figure 1e shows the temperature dependence of resistivity (ρ_{xx}) at $B = 0$ T. The ρ_{xx} shows minimal temperature dependence above T_c, suggesting the incoherent charge transport as often seen in the strongly correlated metals. At T_c, the resistivity shows a kink and steeply decreases at lower temperatures. Figure 2a–t summarizes the magnetization, magnetoresistivity, and Hall resistivity under the magnetic field. The magnetization shows jumps at B_{c1} and B_{c2} below T_c, which are blurred above T_c [see Fig. 2a–e]. The magnetoresistivity also shows anomalies at B_{c1} and B_{c2} in the temperature range 12–18 K. Furthermore, with increasing temperature from 2 K, the negative magnetoresistivity becomes gradually pronounced. In particular, the negative magnetoresistivity is observed up to around 50 K, implying that the short-ranged spin correlation remains even far above T_c.

On the other hand, the Hall resistivity (ρ_{yx}) shows more peculiar temperature and field dependence [See Fig. 2k–o]. At 2 K, ρ_{yx} almost linearly increases as a function of *B* except for a jump at B_{c2}. Since the magnetization is saturated above B_{c2} [see Fig. 2a], the *B*-linear component above B_{c2} is likely attributed to the ordinary Hall effect. The extrapolation of the *B*-linear part to zero magnetic field seems to take a finite value, suggesting the finite contribution from the anomalous Hall effect proportional to *M*. With increasing temperature, the slope of ρ_{yx} above B_{c2} gradually decreases, while that below B_{c2} shows sign change above 12 K. In addition, a peak structure grows around B_{c2} and becomes remarkable at higher temperatures. Above 22 K, the peak shifts to a higher-field region and gradually diminishes while broadening its width. Apparently, such behavior cannot be explained by the conventional anomalous Hall effect proportional to *M*. On the other hand, the ordinary Hall effect can show a peak, given that the carrier mobility is sufficiently high. This is, however, not likely, since the resistivity above T_c is in the incoherent transport regime close to the Ioffe-Regel limit ($\sim 1 \times 10^{-3}\,\Omega$ cm) (see Supplementary Note 1). This suggests the presence of an additional contribution other than the ordinary Hall effect and AHE proportional to *M*. Following the

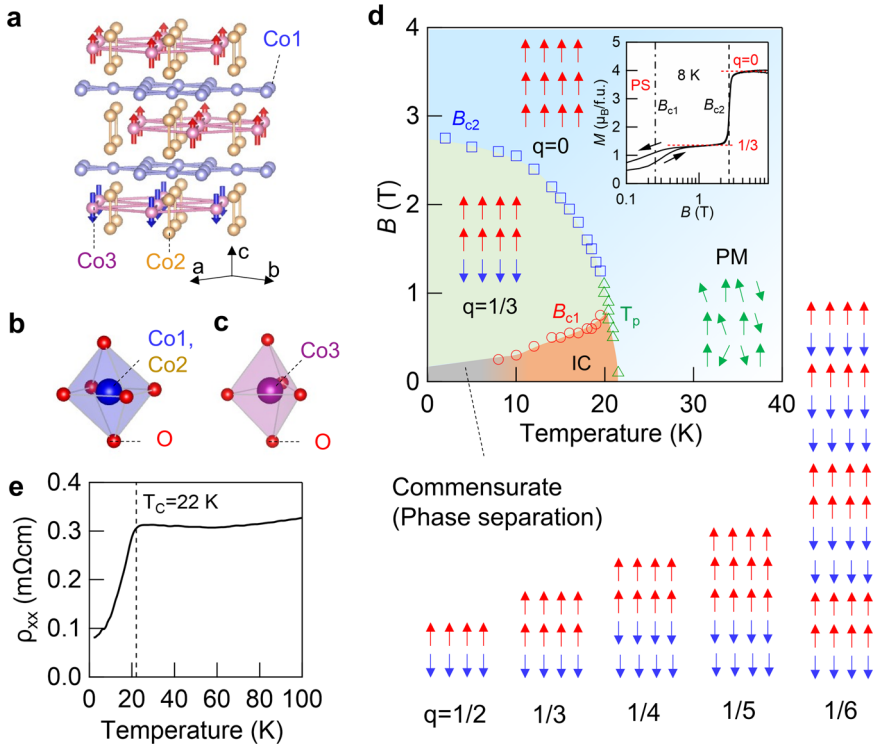

Fig. 1 | Crystal structure and magnetic phase diagram for $SrCo_6O_{11}$. a The illustration of Co-sublattice of $SrCo_6O_{11}$ with up-up-down-type magnetic structure ($q = 1/3$)[50]. Arrows denote the spins on Co3-sites. The primitive vectors *a*, *b*, and *c* are defined in the hexagonal crystal symmetry with space group $P6_3/mmc$. **b**, **c** The illustration of CoO_6-octahedra of Co1 and Co2 and CoO_5-bipyramid of Co3. **d** The magnetic phase diagram in the temperature-magnetic field plane. Arrows denote spins of Co3. Here, *q* represents the wave number of magnetic modulation. Open circles and squares denote the magnetic transition at B_{c1} and B_{c2}, respectively. Open triangles denote the transition temperature (T_p) of the incommensurate (IC) phase or $q = 1/3$-phase determined from the temperature dependence of *M* (See Supplementary Fig. 2d, e). We defined T_p at 0.1 T as T_c (=22 K). The inset shows the magnetization curve at 8 K. The horizontal dotted line denotes the magnetization plateau corresponding to $q = 1/3$- and $q = 0$-phase. **e** Temperature dependence of resistivity at $B = 0$ T.

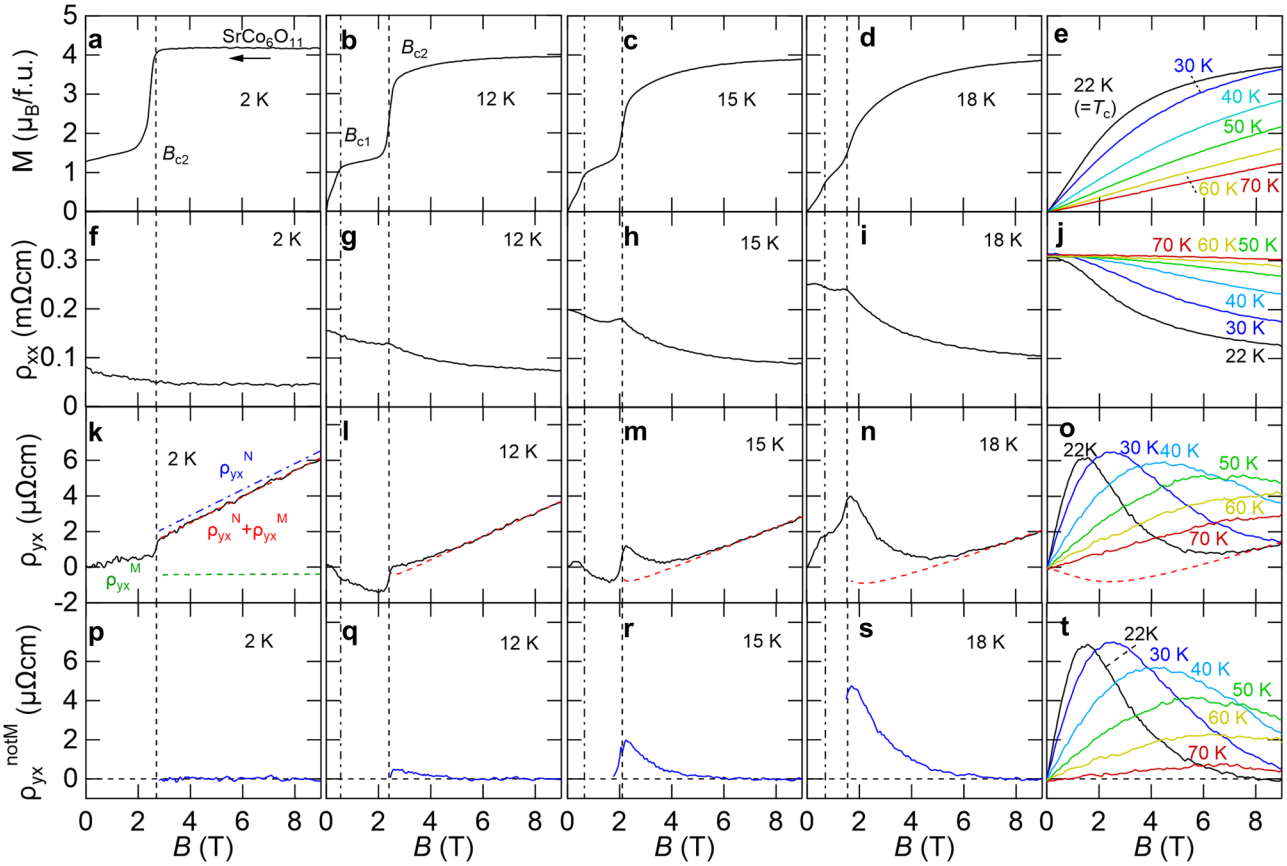

Fig. 2 | Magnetization and electrical transport property for $SrCo_6O_{11}$. a–e The magnetization (M), **f–j** resistivity (ρ_{xx}), **k–o** Hall resistivity (ρ_{yx}), and **p–t** Hall resistivity are not proportional to M (ρ_{yx}^{notM}) for $SrCo_6O_{11}$. The blue dash-dot-line and green dashed line denote the ordinary Hall resistivity (ρ_{yx}^{N}) and anomalous Hall resistivity proportional to M (ρ_{yx}^{M}), respectively. The red dashed curve denotes the $\rho_{yx}^{N}+\rho_{yx}^{M}$ (red dashed curve in **k** denotes the $\rho_{yx}^{N}+\rho_{yx}^{M}$ at 22 K). ρ_{yx}^{N} and ρ_{yx}^{M} are omitted for clarity in **l–o**.

conventional wisdom[7,13,20], we analyzed the Hall resistivity by assuming the following three components,

$$\rho_{yx} = R_N B + S_A \rho_{xx}^{\alpha} M + \rho_{yx}^{notM} \quad (1)$$

The first, second, and third terms represent the ordinary Hall component ($\rho_{yx}^{N} = R_N B$), the anomalous Hall component in proportion to M ($\rho_{yx}^{M} = S_A \rho_{xx}^{\alpha} M$), and the residual component (ρ_{yx}^{notM}), which is neither proportional to B nor to M, respectively. Since the fitting with this model did not uniquely converge in the region below B_{c2} due to the short field range of each magnetic phase [see also Supplementary Note 2], we focus on the results in the forced ferromagnetic/paramagnetic state above B_{c2}. Here, we assumed the exponent $\alpha = 0.4$ for ρ_{yx}^{M} which corresponds to the intrinsic AHE in the incoherent transport regime[1,37]. Although α depends on the transport regime, the analyzed results here did not significantly depend on the choice of α [see Supplementary Note 3]. ρ_{yx}^{N}, ρ_{yx}^{M} and their summation ($= \rho_{yx}^{N} + \rho_{yx}^{M}$) at 2 K are exemplified in Fig. 2k. ρ_{yx} is well reproduced by $\rho_{yx}^{N} + \rho_{yx}^{M}$, resulting in the negligible ρ_{yx}^{notM} [see Fig. 2p]. With increasing temperatures, the difference between ρ_{yx} and $\rho_{yx}^{N} + \rho_{yx}^{M}$ becomes significant especially near B_{c2}, resulting in a peak of ρ_{yx}^{notM} as shown in Fig. 2q–t. Above 30 K, the peak shifts to a higher-field region and gradually diminishes. To visualize this behavior, we show the contour plot of ρ_{yx}^{notM} on the temperature-magnetic field plane in Fig. 3a. It is evident that ρ_{yx}^{notM} is enhanced in the wide temperature-field region near and above T_c, where the magnetization is not fully polarized, namely, the thermal spin fluctuation is remarkable.

To quantitatively compare the temperature dependence of each term, we derived the Hall conductivity $\sigma_{xy}^{M,notM}$ [$= \rho_{yx}^{M,notM}/(\rho_{xx}^2 + \rho_{yx}^2)$]. Figure 3b shows the temperature dependence of σ_{xy}^{M} and σ_{xy}^{notM} at 3 T. Below 10 K, σ_{xy}^{notM} is much smaller than σ_{xy}^{M}. With increasing temperature, σ_{xy}^{notM} increases up to nearby T_c and gradually decreases at higher temperatures, while σ_{xy}^{M} monotonically decreases. Consequently, σ_{xy}^{notM} becomes much larger than σ_{xy}^{M} near and above T_c. It should be noted that the anomalous Hall angle $\rho_{yx}^{notM}/\rho_{xx}$ ($\sim \tan\theta_H$) is more than 0.02 around 24 K at 3 T, which is the highest level among the bulk oxide collinear ferromagnets and antiferromagnets to the best of our knowledge [see Fig. 3c].

Anomalous Hall effect in ferromagnetic $Sr_{0.92}Ba_{0.08}Co_6O_{11}$

Interestingly, the behavior of Hall resistivity is quite different in the system without the magnetic devil's staircases. In the R-type hexaferrite ACo_6O_{11} (A = Ca, Sr, and Ba), the partial substitution of Sr for Ba enhances the interlayer lattice spacing [Supplementary Table 1], which results in the variation of the electronic state and thus interplane RKKY-type magnetic interactions[34,38]. Consequently, a single ferromagnetic transition occurs in the Ba-substituted analog of $SrCo_6O_{11}$ as shown in Fig. 4a, b. Figure 4d–g shows the magnetization, magnetoresistivity, and Hall resistivity for $Sr_{0.92}Ba_{0.08}Co_6O_{11}$ with $T_c = 33$ K [see also Supplementary Fig. 6]. The magnetization curve shows a conventional ferromagnetic behavior at 10 K without any signature of metamagnetic transition. ρ_{xx} shows the negative magnetoresistivity near T_c, similar to the case of $SrCo_6O_{11}$. On the other hand, ρ_{yx} does not show the peak structure as observed in $SrCo_6O_{11}$ even near and above T_c and remains to be negative. As demonstrated in Fig. 4f, ρ_{yx} is well fitted by the sum of ρ_{yx}^{N} and ρ_{yx}^{M} in whole temperature region. In particular, ρ_{yx} is almost governed by ρ_{yx}^{M}, resulting in the small value of ρ_{yx}^{N} and ρ_{yx}^{notM} [see also Supplementary Fig. 6]. As shown in Fig. 4c, g, it is evident that ρ_{yx}^{notM} is much smaller than that for $SrCo_6O_{11}$ in all temperature/field

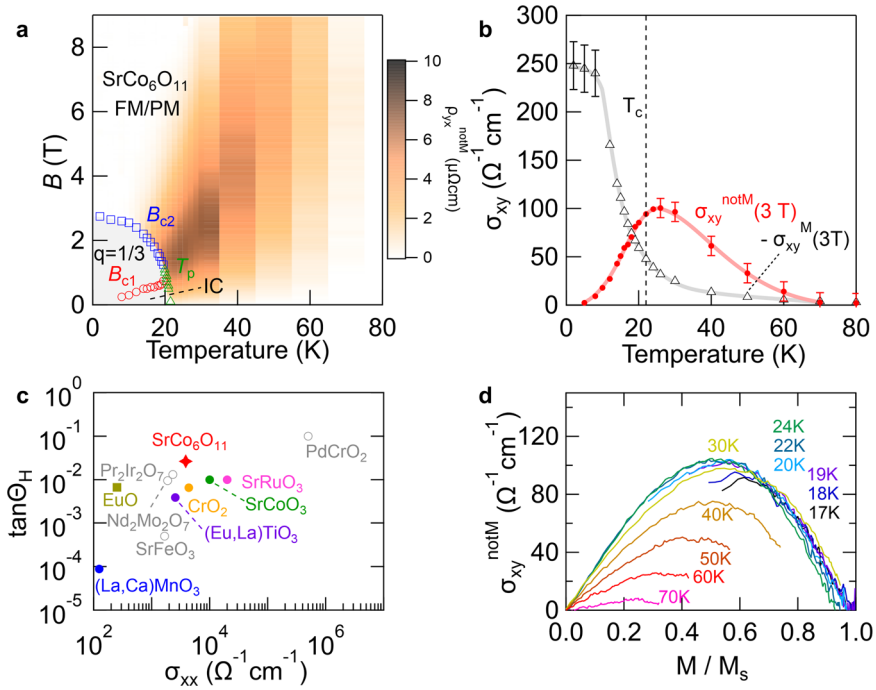

Fig. 3 | Field and temperature dependence of anomalous Hall effect for $SrCo_6O_{11}$. **a** The contour plot of anomalous Hall resistivity not proportional to M (ρ_{xy}^{notM}) on the field-temperature plane. Open circles, squares, and triangles denote the magnetic transition at B_{c1}, B_{c2}, and T_p, respectively. **b** Temperature dependence of σ_{xy}^{notM} (circles) and $-\sigma_{xy}^{M}$ at 3 T (triangles). **c** Anomalous Hall angle ($\tan\theta_H \sim \rho_{yx}^{notM}/\rho_{xx}$) in various bulk oxide ferromagnets (closed circles) and noncollinear magnets (open circles)[1,51–58]. **d** Anomalous Hall conductivity not proportional to magnetization (σ_{xy}^{notM}) as a function of normalized magnetization (M/M_s) with M_s being the magnetization at 2 K and 9 T.

regions. These results suggest that the remarkable AHE is triggered by the spin fluctuation inherent to the magnetic devil's staircase.

Disordering dependence of anomalous Hall effect

The insight into the mechanism of AHE is often acquired from the scaling relation between σ_{xx} and σ_{xy}^{notM}. To systematically change σ_{xx} near T_c without substantially changing the magnetic state, we prepared two sample sets of $Sr_{1-x}(Ca_{1-\delta}Ba_\delta)_xCo_6O_{11}$ with $x = 0.02$ (set A: $\delta = 0.31$ and set B: $\delta = 0.25$); the co-doping of Ba and Ca enhances the non-magnetic lattice disorder while keeping the lattice constants and magnetic devil's staircase [see Supplementary Tables 1, 2 and Supplementary Fig. 7]. As shown in Fig. 5a, the resistivity for the doped system is enhanced compared with the undoped system, while the kink at T_c remains to be observed. The inset to Fig. 5a shows the ρ_{yx} at several temperatures above T_c. ρ_{yx} shows a peak similar to the case of $x = 0$ [see also Supplementary Figs. 7 and 8]. We derived σ_{xy}^{notM} as in the case of undoped systems and plotted the peak value at several temperatures near T_c (22 - 26 K) for several samples in Fig. 5b. The peak of σ_{xy}^{notM} seems to be scaled to σ_{xx}^2.

Discussion

In general, there are several possible mechanisms for the AHE induced by thermal spin fluctuation. A possibility is the conventional extrinsic AHE from skew scattering or side-jump mechanism. σ_{xy} of skew scattering mechanism (side-jump mechanism) is known to be proportional to σ_{xx} (σ_{xx}^0)[1]. Moreover, the conventional extrinsic AHE is usually much smaller than the intrinsic AHE, that is, the typical anomalous Hall angle ($\tan\theta_H$) is less than 0.01. Therefore, this may not be likely for the present case [see also Fig. 3c and Fig. 5b]. Another possibility is the AHE due to the vector spin chirality $S_i \times S_j$[39–41]. This mechanism, however, requires strong crystalline inhomogeneity or inversion-symmetry breaking. Since the crystal structure is derived to be centrosymmetric[29], this may be also unlikely in the present case. The most plausible mechanism is the three-spin correlation process related to the SSC. In this case, the large Hall signal that is not proportional to M can be induced by a chiral spin texture or local correlation[8–11,26,27,42–44]. This often manifests itself as the anomalous Hall signal which becomes remarkable in the partially spin-polarized state near the transition temperature in ferromagnets. In Fig. 3d, we plot σ_{xy}^{notM} as a function of magnetization normalized by the saturated magnetization M_s i.e. magnetization at 2 K and 9 T. σ_{xy}^{notM} near and above T_c is commonly maximal at $M/M_s \sim 0.5$, as in the case of other magnets showing the thermally induced SSC[21,26].

To explore whether the thermal spin fluctuation can generate the finite SSC in $SrCo_6O_{11}$, we theoretically calculated the SSC using Monte Carlo simulation. To this end, we consider a Kondo lattice model with conduction electron layers [Co1] sandwiched by the layers of classical moments on *AB*-stacked bilayer triangular lattice [Co(3)] [see Fig. 6a, b]; the itinerant electrons interact with the localized moments by the inter-site exchange interaction. The effective spin model for the localized moments on the *AB*-stacked triangular lattice is assumed to be

$$H = -J_0 \sum_{\langle i,j\rangle_{xy}} \boldsymbol{S}_i \cdot \boldsymbol{S}_j - \sum_{\langle i,j\rangle_{xy}} D_{ij}\hat{z} \cdot \left(\boldsymbol{S}_i \times \boldsymbol{S}_j\right) - J_1 \sum_{\langle i,j\rangle_z} \boldsymbol{S}_i \cdot \boldsymbol{S}_j - J_2 \sum_{\langle i,j\rangle_z} \boldsymbol{S}_i \cdot \boldsymbol{S}_j - K_z \sum_i \left(S_i^z\right)^2 - h_z \sum_i S_i^z, \quad (2)$$

which is inspired by the ANNNI model[35,36]. Here, $\boldsymbol{S}_i$ is the localized Heisenberg spin on the i th site, J_0, J_1 and J_2 are in-plane nearest neighbor-, out-of-plane nearest-neighbor-, and out-of-plane second-nearest-neighbor-exchange interactions, respectively. Considering the local symmetry for the intralayer Co(3)- Co(3) bond, the in-plane Dzyaloshinskii-Moriya (DM) interaction D_{ij} is assumed. K_z and h_z are the easy-axis anisotropy and external magnetic field along z-axis (c-axis), respectively. For the calculation, we assumed $J_1 = J_0 = 1/3$, $-1 \le J_2 \le 0$, $K_z = 10$ and $D_{ij} = 1/6$. The statistical property of this model is studied using the Monte Carlo method with the heat bath local update method.

The magnetic phase diagram at $h_z = 0$ is shown in Fig. 6c. For $J_2/3J_1 = 0$, a ferromagnetic phase with spontaneous magnetization along z-axis emerges at $T = 2.3J_0$. On the contrary, for $J_2/3J_1 = -1$, a number of collinear antiferromagnetic orderings with easy-axis along z-direction successively emerge as the temperature decreases; the phase with modulation vector $q = 7/32$ parallel to the z-axis appears at $T = 2.3J_0$, that with $q = 15/64$ at around $T = 1.8J_0$ and that with $q = 1/4$ at around $T = 1.3J_0$, similar to that of the Ising spin model[45]. By applying the magnetic field, these antiferromagnetic phases turn into the field-forced ferromagnetic phase. As shown in Fig. 6d, the field-induced phase transition manifests itself as a jump of magnetization around $h_z = J_0$ at low temperatures. At high

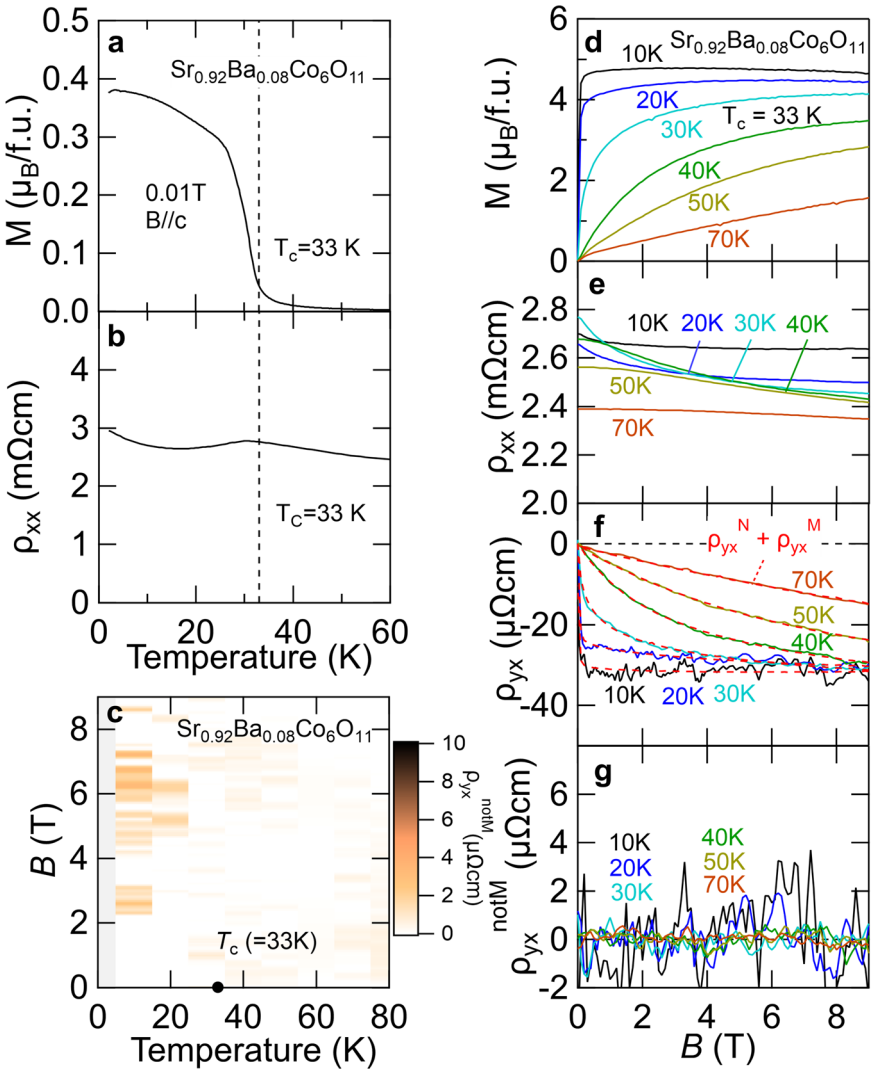

Fig. 4 | The magnetization, resistivity, and Hall resistivity for $Sr_{0.92}Ba_{0.08}Co_6O_{11}$. a, **b** Temperature dependence of magnetization (M) measured at $B = 0.01$ T and resistivity (ρ_{xx}) at $B = 0$ T. **c** The contour plot of anomalous Hall resistivity not proportional to M (ρ_{xy}^{notM}) on the field-temperature plane. The closed circle denotes T_c of ferromagnetic ordering. **d**–**g** The magnetization (M), resistivity (ρ_{xx}), Hall resistivity (ρ_{yx}), and Hall resistivity are not proportional to M (ρ_{yx}^{notM}), respectively.

temperatures above the antiferromagnetic transition temperature, the jump is replaced by a crossover. The calculated result is consistent with the experimental result about the appearance of temperature/field-induced transitions among magnetic phases with different q.

To study the temperature/field dependence of SSC, we focus on the thermal average of SSC for three spins on sites i, j, k

$$\chi = \left\langle \boldsymbol{S}_i \cdot \left(\boldsymbol{S}_j \times \boldsymbol{S}_k \right) \right\rangle = \frac{1}{Z} Tr \left[\sum_{\langle i,j,k \rangle} \boldsymbol{S}_i \cdot \left(\boldsymbol{S}_j \times \boldsymbol{S}_k \right) \exp(-\beta \mathrm{H}) \right] \quad (3)$$

where the sum over i, j, k is the sum over three nearest-neighbor spins on the two adjacent Co3 layers sandwiching the conduction layer [Fig. 6a, b]. Here, $\beta = 1/k_B T$, and Z is the partition function. Note that, for a translationally symmetric triangular lattice, the chirality of an upward triangle is exactly the opposite of the downward triangles. Hence, the SSC of three nearest-neighbor spins within a triangular layer does not contribute to the AHE. Therefore, we consider the SSC of three spins on two adjacent layers sandwiching a conduction layer. An example of the three spins $\boldsymbol{S}_i$ ($i = 1,2,3$) is shown in Fig. 6a, b, in which $\boldsymbol{S}_3$ is on a different layer from $\boldsymbol{S}_1$ and $\boldsymbol{S}_2$. The thermal average of SSC is shown in Fig. 6e, in which SSC is small in the antiferromagnetic phase in the low field and low-temperature region. On the contrary, it is enhanced in the forced ferromagnetic/paramagnetic phase in the high-temperature region. In particular, the peak field of a thermal average of SSC increases with increasing temperature. This suggests that the conduction electrons of Co(1)-site acquire the finite SSC from the thermal fluctuation of Co(3)-spin in the present material, which is particularly enhanced above the magnetic transition temperature.

Finally, we discuss the mechanism of AHE from the thermally induced SSC. In the scheme of Berry curvature in momentum space, σ_{xy} is predicted to be proportional to σ_{xx}^0, which is not consistent with the present result [see Fig. 5b]. The result also seems to be slightly deviate from $\sigma_{xx}^{1.6}$-law[37]. On the contrary, the multiple skew scattering mechanism, topological Hall effect, and orbital Berry phase mechanism propose the σ_{xx}^2-law[10,19,46,47]. Considering that the large σ_{xy}^{notM} remains even at high temperatures where the spin correlation length would be significantly reduced, the multiple skew scattering may be most likely.

It should be noted that the large Hall effect remaining even far above the magnetic transition temperature is observed in the magnetic semiconductor EuAs and Skyrmion magnets $Gd_3Ru_4Al_{12}$[20,48]. The common feature of these materials is that the long-range ordered phase below transition temperature is characterized by the noncoplanar spin structure. This is in contrast with the present material with the collinear antiferromagnetic ordering. In collinear antiferromagnets with devil's staircase transition, it has been known that the solitonic or cluster-like spin defects such as domain walls thermally proliferate and diffuse near and above T_c[35,36,49]. Although such spin excitation has not been accurately captured by the current theoretical calculation, the spin-flip excitation is presumed to cause the large-angle transient noncoplanar spin texture, resulting in the SSC-related skew scattering of electrons.

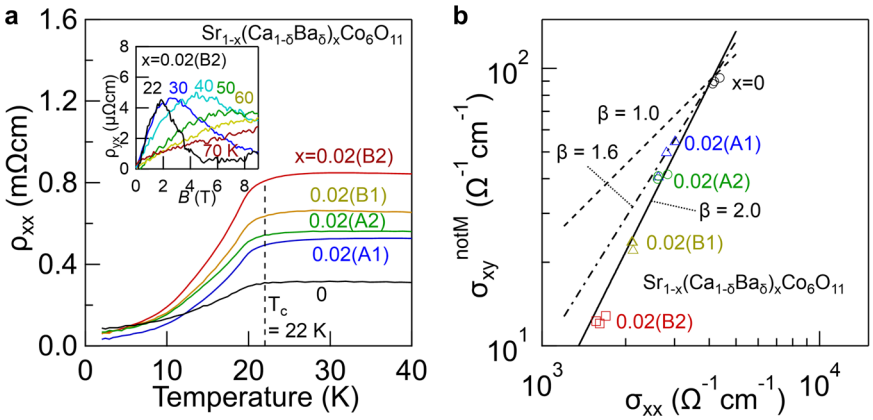

Fig. 5 | The scaling relation between σ_{xx} and σ_{xy}^{notM}. **a** Temperature dependence of resistivity for two set of $Sr_{1-x}(Ca_{1-\delta}Ba_\delta)_xCo_6O_{11}$ with $x = 0.02$ (A1, A2, B1 and B2). Inset shows ρ_{yx} for sample B2. **b** The peak value of σ_{xy}^{notM} near T_c (22–26 K) plotted as a function of σ_{xx}. The dashed, dash-dot, and solid lines denote $\sigma_{xy}^{notM} \propto \sigma_{xx}^{\beta}$ with $\beta = 1.0$, 1.6, and 2.0, respectively.

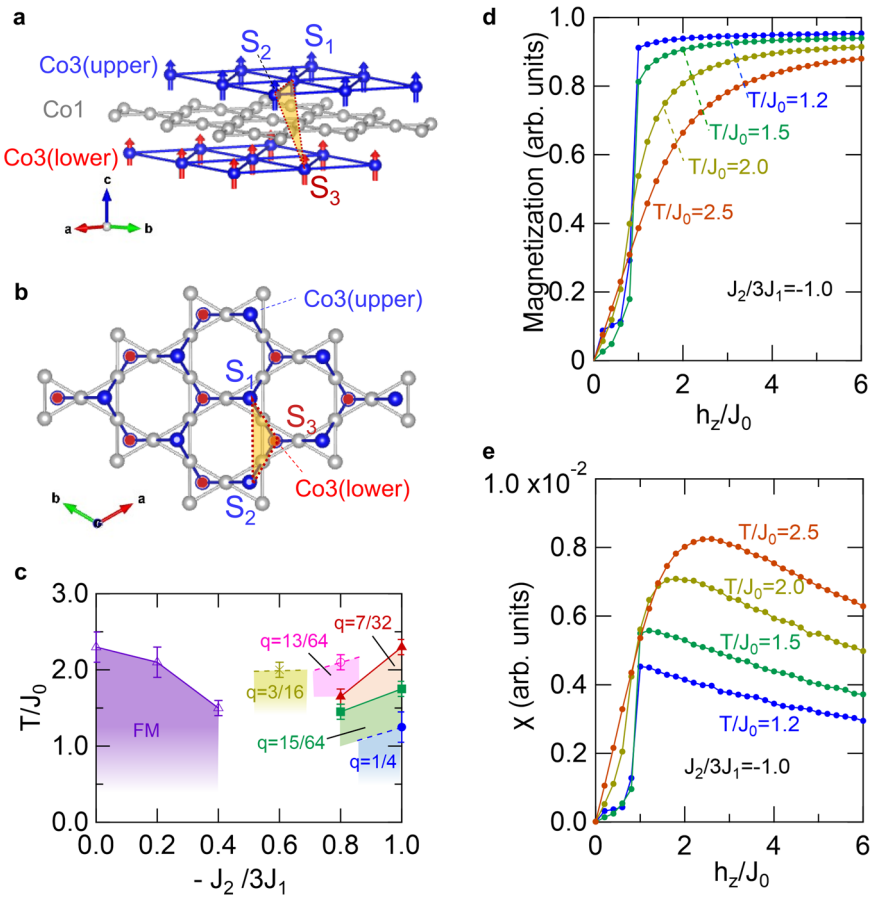

Fig. 6 | Monte Carlo simulation of scalar-spin chirality. **a** Side view and **b** top view of *AB*-stacked triangular lattice of Co3 and Kagome layer of Co1. The yellow triangle with a dotted edge denotes an example of a triangle considering the SSC. The in-plane solid line of the Co3 triangular lattice denotes the magnetic bond with Dzyaloshinskii-Moriya (DM) interaction. **c** The magnetic phase diagram on the temperature vs. $-J_2/3J_1$ plane. **d**, **e** Magnetization and thermal average of scalar spin chirality for the nearest-neighbor triangles. The results in **c**–**e** are for $N = 16 \times 16 \times 64$ system size with $J_0 = 1/3$, $J_1 = 1/3$, $D = 1/6$, $K_z = 10$.

In this paper, we show that the collinear antiferromagnetic metal $SrCo_6O_{11}$ exhibits the large anomalous Hall effect (AHE) due to the spin fluctuation of the devil's staircase-type transition by means of transport measurement and theoretical calculation. In particular, the maximum of anomalous Hall angle exceeds 0.02, which is the highest level among the known bulk oxide collinear ferromagnets/antiferromagnets. The AHE not scaled to the magnetization becomes remarkably near and above the transition temperature (T_c) but vanishes in the field-induced fully spin-polarized state. Furthermore, such thermally induced AHE is not clearly observed in the ferromagnetic $Sr_{0.92}Ba_{0.08}Co_6O_{11}$ without the devil's staircase transition. We also found that the anomalous hall conductivity not scaled to magnetization (σ_{xy}^{notM}) is quadratically scaled to electrical conductivity, i.e., $\sigma_{xy}^{notM} \propto \sigma_{xx}^{2}$. These results imply that the thermally induced proliferation of solitonic/cluster-like spin defects inherent to the magnetic devil's staircase enhances the scalar-spin-chirality skew scattering of electrons, yielding the large AHE. This work demonstrates that the large anomalous Hall effect comparable or larger than the well-known Berry curvature mechanism can be induced above the transition temperature in a collinear antiferromagnetic metal, paving a new route for high-temperature paramagnetic spintronics function such as efficient thermoelectric energy harvesting.

Methods

Sample preparation and characterization

Single crystals of *R*-type hexaferrite $SrCo_6O_{11}$ were grown under pressure by means of the cubic-anvil-type facility. The starting materials are $Sr_3Co_2O_{7-\delta}$,

$Sr(OH)_2 \cdot 8H_2O$, and $KClO_4$ mixed in a ratio of 8:1:3. The mixture was sealed in Pt capsule and was heated up to 840 ∘C under 2 GPa. It was kept there for 10 min and then quenched to room temperature. The typical size of a crystal is about $0.3 \times 0.3 \times 0.1$ mm with the shape of a hexagonal plate normal to the c-axis. Supplementary Fig. 1 shows the photograph of the sample. The unit cell of samples is determined by the single crystalline X-ray diffraction at room temperature (see Supplementary Table 1). Single crystalline samples of $Sr_{0.92}Ba_{0.08}Co_6O_{11}$ and $Sr_{1-x}(Ca_{1-\delta}Ba_\delta)_xCo_6O_{11}$ $x = 0.02$ (set A: $\delta = 0.31$ and set B: $\delta = 0.25$) are grown by similar conditions. For the latter, two series of samples (A and B) were prepared (see Supplementary Table 1 and 2). Sr-, Ca- and Ba-concentration are determined by the energy dispersive X-ray spectroscopy (EDX) analysis and scanning electron microscopy (SEM).

Measurement of resistivity, Hall resistivity, and magnetization

Measurements of resistivity and Hall resistivity were performed by standard four-terminal geometry with an indium electrode. The measurements were done by using the Physical Property Measurement System (Quantum Design) from 2 K to 300 K under the magnetic field up to 9 T. The magnetization measurements were performed by using the Dynacool System equipped with the VSM option from 2 K to 300 K under the magnetic field up to 9 T. The several samples with different shapes show nearly identical magnetization profiles, suggesting that the demagnetization factor is not significant. The magnetization measurement was performed for samples for which the transport property was measured.

Monte Carlo simulation

The magnetic phase diagram and field dependence were calculated using a Monte Carlo simulation with the standard heat-bath update method. The physical quantities were calculated using 120,000 MC steps after 20,000 steps of relaxation. The MC results were split into 6 bins for estimating the statistical error. All calculations were performed using an on-premise PC cluster at the Tokyo Institute of Technology.

Data availability

All data needed to evaluate the conclusions in the paper are present in the paper and/or the supplementary Information. Additional data requests should be addressed to the corresponding authors.

Code availability

The codes used during the current study are available from the corresponding author upon reasonable request.

Received: 18 December 2023; Accepted: 24 April 2024;
Published online: 17 May 2024

References

1. Nagaosa, N., Sinova, J., Onoda, S., MacDonald, A. H. & Ong, N. P. Anomalous Hall effect.Rev. *Mod. Phys.* **82**, 1539 (2010).
2. Schulz, T. et al. Emergent electrodynamics of skyrmions in a chiral magnet. *Nat. Phys.* **8**, 301 (2012).
3. Feng, Z. et al. An anomalous Hall effect in altermagnetic ruthenium dioxide. *Nat. Electron.* **5**, 735 (2022).
4. Wang, M. et al. Emergent zero-field anomalous Hall effect in a reconstructed rutile antiferromagnetic metal. *Nat. Commun.* **14**, 8240 (2023).
5. Nakatsuji, S., Kiyohara, N. & Higo, T. Large anomalous Hall effect in a non-collinear antiferromagnet at room temperature. *Nature* **527**, 212 (2015).
6. Kotegawa, H. et al. Large anomalous Hall effect and unusual domain switching in an orthorhombic antiferromagnetic material NbMnP. *npj Quant. Mater.* **8**, 56 (2023).
7. Neubauer, A. et al. Topological hall effect in the A phase of MnSi. *Phys. Rev. Lett.* **102**, 186602 (2009).
8. Ohgushi, K., Murakami, S. & Nagaosa, N. Spin anisotropy and quantum Hall effect in the kagome lattice: Chiral spin state based on a ferromagnet. *Phys. Rev. B* **62**, R6065 (2000).
9. Taguchi, Y., Oohara, Y., Yoshizawa, H., Nagaosa, N. & Tokura, Y. Spin chirality, berry phase, and anomalous Hall effect in a frustrated ferromagnet. *Science* **291**, 2573 (2001).
10. Tatara, G. & Kawamura, H. Chirality-driven anomalous Hall effect in weak coupling regime. *J. Phys. Soc. Jpn* **71**, 2613 (2002).
11. Onoda, M., Tatara, G. & Nagaosa, N. Anomalous Hall effect and skyrmion number in real and momentum spaces. *J. Phys. Soc. Jpn.* **73**, 2624 (2004).
12. Ye, J. et al. Berry phase theory of the anomalous Hall effect: application to colossal magnetoresistance manganites. *Phys. Rev. Lett.* **83**, 3737 (1999).
13. Raju, M. et al. Colossal topological Hall effect at the transition between isolated and lattice-phase interfacial skyrmions. *Nat. Commun.* **12**, 2758 (2021).
14. Matsui, A., Nomoto, T. & Arita, R. Skyrmion-size dependence of the topological Hall effect: A real-space calculation. *Phys. Rev. B* **104**, 174432 (2021).
15. Maccariello, D. et al. Electrical detection of single magnetic skyrmions in metallic multilayers at room temperature. *Nat. Nanotechnol.* **13**, 233 (2018).
16. Mizuta, Y. P. & Ishii, F. Large anomalous Nernst effect in a skyrmion crystal. *Sci. Rep.* **6**, 28076 (2016).
17. Smit, J. The spontaneous hall effect in ferromagnetics II. *Phys. Ther.* **24**, 39–51 (1958).
18. Berger, L. Side-jump mechanism for the Hall effect of ferromagnets. *Phys. Rev. B* **2**, 4559–4566 (1970).
19. Ishizuka, H. & Nagaosa, N. Spin chirality induced skew scattering and anomalous Hall effect in chiral magnets. *Sci. Adv.* **4**, eaap9962 (2018).
20. Uchida, M. et al. Above-ordering-temperature large anomalous Hall effect in a triangular-lattice magnetic semiconductor. *Sci. Adv.* **7**, eabl5381 (2021).
21. Kolincio, K. K. et al. Large Hall and Nernst responses from thermally induced spin chirality in a spin-trimer ferromagnet. *Proc. Natl Acad. Sci.* **118**, e2023588118 (2021).
22. Ghimire, N. J. et al. Competing magnetic phases and fluctuation-driven scalar spin chirality in the kagome metal YMn_6Sn_6. *Sci. Adv.* **6**, 2680 (2020).
23. Cheng, Y., Yu, S., Zhu, M., Hwang, J. & Yang, F. Evidence of the topological Hall effect in Pt/antiferromagnetic insulator bilayers. *Phys. Rev. Lett.* **123**, 237206 (2019).
24. Wang, W. et al. Spin chirality fluctuation in two-dimensional ferromagnets with perpendicular magnetic anisotropy. *Nat. Mater.* **18**, 1054–1059 (2019).
25. Checkelsky, J. G., Lee, M., Morosan, E., Cava, R. J. & Ong, N. P. Anomalous Hall effect and magnetoresistance in the layered ferromagnet $Fe_{1/4}TaS_2$: the inelastic regime. *Phys. Rev. B* **77**, 014433 (2008).
26. Chun, S. H., Salamon, M. B., Lyanda-Geller, Y., Goldbart, P. M. & Han, P. D. Magnetotransport in manganites and the role of quantal phases: theory and experiment. *Phys. Rev. Lett.* **84**, 757 (2000).
27. Matl, P. et al. Hall effect of the colossal magnetoresistance manganite $La_{1-x}Ca_xMnO_3$. *Phys. Rev. B* **57**, 10248 (1998).
28. Hua, E. et al. Ru-doping-induced spin frustration and enhancement of the room-temperature anomalous Hall effect in $La_{2/3}Sr_{1/3}MnO_3$ Films. *Adv. Mater.* **34**, 2206685 (2022).
29. Ishiwata, S., Wang, D., Saito, T. & Takano, M. High-pressure synthesis and structure of $SrCo_6O_{11}$: pillared kagome lattice system with a 1/3 magnetization plateau. *Chem. Mater.* **17**, 2789 (2005).
30. Saito, T. et al. Neutron diffraction study of a layered cobalt oxide $SrCo_6O_1$. *1 J. Magn. Magn. Mater.* **310**, 1584 (2007).
31. Mukuda, H. et al. ^{59} Co-NMR probe for stepwise magnetization and magnetotransport in $SrCo_6O_{11}$ with metallic Kagome layer and

triangular lattice with local. *Moments, J. Phys. Soc. Jpn.* **75**, 094715 (2006).
32. Lee, C., Whangbo, M.-H. & Villesuzanne, A. On the electronic structure required for the uniaxial magnetic properties of the magnetic metal $SrCo_6O_{11}$. *Chem. Mater.* **19**, 2712–2714 (2007).
33. Ishiwata, S. et al. Two-staged magnetoresistance driven by the Ising-like spin sublattice in $SrCo_6O_{11}$. *Phys. Rev. Lett.* **98**, 217201 (2007).
34. Matsuda, T. et al. Observation of a devil's staircase in the novel spin-valve system $SrCo_6O_{11}$. *Phys. Rev. Lett.* **114**, 236403 (2015).
35. Bak, P. & von Boehm, J. Ising model with solitons, phasons, and "the devil's staircase". *Phys. Rev. B* **21**, 5297 (1980).
36. Selke, W. The ANNNI model—theoretical analysis and experimental application. *Phys. Rep.* **170**, 213 (1988).
37. Onoda, S., Sugimoto, N. & Nagaosa, N. Intrinsic versus extrinsic anomalous Hall effect in ferromagnets. *Phys. Rev. Lett.* **97**, 126602 (2006).
38. Yamada, I., Toda, F., Kawaguchi, S. & d'Astuto, M. Various magnetic states for novel layered cobalt oxides $CaCo_6O_{11}$ and $BaCo_6O_{11}$ M. *Mater. Chem. Front.* **3**, 26962701 (2019).
39. Taguchi, K. & Tatara, G. Anomalous Hall conductivity due to vector spin chirality in the weak coupling regime. *Phys. Rev. B* **79**, 054423 (2009).
40. Ishizuka, H. & Nagaosa, N. Impurity-induced vector spin chirality and anomalous Hall effect in ferromagnetic metals. *N. J. Phys.* **20**, 123027 (2018).
41. Lux, F. R., Freimuth, F., Blugel, S. & Mokrousov, Y. Chiral Hall effect in noncollinear magnets from a cyclic cohomology approach. *Phys. Rev. Lett.* **124**, 096602 (2020).
42. Fujishiro, Y. et al. Giant anomalous Hall effect from spin-chirality scattering in a chiral magnet. *Nat. Commun.* **12**, 317 (2021).
43. Ishizuka, H. & Nagaosa, N. Large anomalous Hall effect and spin Hall effect by spin-cluster scattering in the strong-coupling limit. *Phys. Rev. B.* **103**, 235148 (2021).
44. Denisov, K. S., Rozhansky, I. V., Averkiev, N. S. & Lahderanta, E. General theory of the topological Hall effect in systems with chiral spin textures. *Phys. Rev. B* **98**, 195439 (2018).
45. Murtazaev, A. K. & Ibaev, Zh. G. Critical Properties of the Anisotropic Ising Model with Competitive Interactions. *J. Exp. Theoret. Phys.* **113**, 106–112 (2011).
46. Tomizawa, T. & Kontani, H. Anomalous Hall effect in the t_{2g} orbital kagome lattice due to noncollinearity: Significance of the orbital Aharonov-Bohm effect. *Phys. Rev. B* **80**, 100401 (2009).
47. Nakazawa, K., Bibes, M. & Kohno, H. Topological Hall effect from strong to weak coupling. *J. Phys. Soc. Jpn.* **87**, 033705 (2018).
48. Kolincio, KamilK. et al. Kagome Lattice promotes chiral spin fluctuations. *Phys. Rev. Lett.* **130**, 136701 (2023).
49. Kamiya, Y. & Batista, C. D. Formation of magnetic microphases in $Ca_3Co_2O_6$. *Phys. Rev. Lett.* **109**, 067204 (2012).
50. Momma, K. & Izumi, F. VESTA 3 for three-dimensional visualization of crystal, volumetric and morphology data. *J. Appl. Cryst.* **44**, 1272–1276 (2011).
51. Ishiwata, S. et al. Versatile helimagnetic phases under magnetic fields in cubic perovskite $SrFeO_3$. *Phys. Rev. B* **84**, 054427 (2011).
52. Ohuchi, Y. et al. Photoinduced sign inversion of the anomalous Hall effect in EuO thin films. *Phys. Rev. B* **89**, 121114 (2014).
53. Takahashi, K. S. et al. Anomalous Hall effect derived from multiple Weyl nodes in high-mobility $EuTiO_3$ films. *Sci. Adv.* **4**, eaar7880 (2018).
54. Yanagihara, H. & Salamon, M. B. Skyrmion strings and the anomalous Hall effect in CrO_2. *Phys. Rev. Lett.* **89**, 187201 (2002).
55. Zhang, D. et al. Anomalous Hall effect and spin fluctuations in ionic liquid gated $SrCoO_3$ thin films. *Phys. Rev. B.* **97**, 184433 (2018).
56. Mathieu, R. Scaling of the anomalous Hall effect in $Sr_{1-x}Ca_xRuO_3$. *Phys. Rev. Lett.* **93**, 016602 (2004).
57. Machida, Y. et al. Unconventional anomalous Hall effect enhanced by a noncoplanar spin texture in the frustrated Kondo lattice $Pr_2Ir_2O_7$. *Phys. Rev. Lett.* **98**, 057203 (2007).
58. Ok, J. M. et al. Quantum oscillations of the metallic triangular-lattice antiferromagnet $PdCrO_2$. *Phys. Rev. Lett.* **111**, 176405 (2013).

Acknowledgements

The authors thank F. Kagawa, M. Wang, and T. Koyano for fruitful discussion and technical support for the transport measurements. MANA is supported by the World Premier International Research Center Initiative (WPI) of MEXT, Japan. This work was supported by a Japan Society for the Promotion of Science KAKENHI (No. 21K18813, No. 22H01177, No. 22H00343, No. 23H04871, and No. 22H04601) from the MEXT, by the Kazuchika Okura Memorial Foundation (No. 2022-11) and by the Nippon Sheet Glass Foundation for Materials Science and Engineering, Japan.

Author contributions

J.F. conceived the project. N.A., Y.H., Y.T., and K.Y. grew the single crystalline $SrCo_6O_{11}$ and performed the characterization with the help of S.I. N.A., Y.H., and Y.K. conducted the transport/magnetization measurement and analyzed the data. H.I. and T.T. performed the numerical calculation and ab initio calculation. J.F., S.I., and H.I. wrote the manuscript with contributions from all authors.

Competing interests

The authors declare no competing interests.

Additional information

Supplementary information The online version contains supplementary material available at https://doi.org/10.1038/s41535-024-00653-3.

Correspondence and requests for materials should be addressed to Jun Fujioka.